Robust determination of relaxation times spectra of long-time multirelaxation processes

Robust determination of relaxation times spectra of long-time multirelaxation processes

J. Kober,[1] M. Scalerandi,[2] and D. Gabriel[1]
[1]*Institute of Thermomechanics of the Czech Academy of Sciences, Prague 18200, Czech Republic*
[2]*DISAT, Condensed Matter Physics and Complex Systems Institute, Politecnico di Torino 10129, Italy*

(Received 9 June 2022; revised 11 October 2022; accepted 27 February 2023; published 14 March 2023)

Long-time relaxation processes occur in numerous physical systems. They are often regarded as multirelaxation processes, which are a superposition of exponential decays with a certain distribution of relaxation times. The relaxation times spectra often convey information about the underlying physics. Extracting the spectrum of relaxation times from experimental data is, however, difficult. This is partly due to the mathematical properties of the problem and partly due to experimental limitations. In this paper, we perform the inversion of time-series relaxation data into a relaxation spectrum using the singular value decomposition accompanied by the Akaike information criterion estimator. We show that this approach does not need any *a priori* information on the spectral shape and that it delivers a solution that consistently approximates the best one achievable for given experimental dataset. On the contrary, we show that the solution obtained imposing an optimal fit of experimental data is often far from reconstructing well the distribution of relaxation times.

DOI: 10.1103/PhysRevE.107.035302

I. INTRODUCTION

Long-time relaxation is common to numerous physical processes: elastic slow dynamics in nonclassical media [1,2], stress-induced conditioning [3], dispersion in nematic liquid crystals [4,5], magnetization processes in nanoparticles [6], relaxation in glass forming liquids [7,8], macromolecules relaxation [9,10], and many others. A lot of the interest in these kind of processes stems from geophysical applications [11–15].

The description and understanding of the long-time relaxation depends strongly on the underlying physics. Albeit other approaches to describe these phenomena have been proposed [16–18], regarding them as a multirelaxation process seems to be the most common. Multirelaxation is a combination of exponential relaxation processes with different time constants [9,11,19,20], which create the spectrum of relaxation times. It has been shown for certain physical systems that the properties of relaxation times spectra can correlate with typical space scales present in the system, e.g., pore radii [9], grain sizes [21,22], or correlation lengths [23].

In order to analyze the spectrum of relaxation times, an inversion of the relaxation curve must be done, i.e., time-series experimental data need to be interpreted by means of a distribution function of relaxation times [24]. The inversion procedure is complex for two main reasons. First, the quality of experimental data is usually limited by the fact that relaxation times often span over up to six decades and both short and long times are important. It can be challenging to sample the relaxation curve sufficiently in all timescales and at the same time to minimize the presence of noise. Second, the mathematical inversion is a not well-posed problem. As a consequence, the inversed relaxation spectrum describing the phenomenon might not be unique [7,20].

Different approaches have been proposed to derive the relaxation-time spectrum distribution: Using a finite, discrete basis of exponentials for the inversion [19], proposing an "ad hoc" continuous function to describe the spectrum motivated by physical considerations [1,25], or combining the two approaches and proposing a continuous function derived by fitting data with a discrete exponential basis [20]. More often, a general analytical approach based on the inversion of the matrix of exponentials is used [4]. Due to the high dimension of the exponential basis matrix, the inverse solution is numerically unstable and highly dependent on the noise in time-series data. Therefore, an approximate inverted matrix needs to be computed using the singular value decomposition (SVD) where the rank order is truncated based on the properties of data to be inverted [26,27].

Several approaches have been proposed to estimate the optimal truncated rank order of SVD, such as using the maximum-entropy criterion [28] or Tikhonov [29] or non-convex [30] regularization, often tailored to specific problems and needing an *a priori* information about the solution to be found. These approaches, however, partly fail when long-time relaxation phenomena are at play. In particular, the choice of the optimal truncated rank consists in separating the ensemble of SVD solutions as a function of rank order into two subsets. For large rank of the SVD matrix, overfitting occurs (resulting in fitting experimental noise); for low rank of the SVD underfitting occurs (the basis is insufficient to correctly fit data). Thus the problem becomes that of defining a criterion to separate rank intervals in which different models of these subsets apply. It could be solved using the Akaike information criterion (AIC) [31–34], which found several applications in extracting the subset of data fitting a model from noisy signals [35–38].

We test the approach by inverting synthetic data. After having defined a distribution function of relaxation times and having derived synthetic data using a multirelaxation formulation (Sec. II), we invert data using the SVD approach combined with the AIC, as introduced in Sec. III. Albeit the

obtained solution approximates the best one achievable for a given dataset, still it contains important deviations in the estimated spectrum of relaxation times with respect to the exact one (Sec. IV), which has to be taken into consideration when interpreting results of an experiment (Sec. V). We also discuss the "empirical" robustness of the approach (not in a statistical sense) by proving the efficiency is independent from the experimental conditions or the properties of the solution to be found, at least up to a certain extent.

II. THEORETICAL DETERMINATION OF THE DISTRIBUTION OF RELAXATION TIMES

A. Multirelaxation processes

Multirelaxation processes are observed in a wide variety of physical systems. The evolution of the relevant physical variable over time $y(t)$ can be described as the superposition of relaxation processes with relaxation times τ distributed according to a given distribution function $F(\tau)$, from now on called τ spectrum:

$$y(t) = \int_0^\infty F(\tau) e^{-t/\tau} d\tau. \tag{1}$$

Often the τ spectrum spans up to six decades while both short and long times are important in the process. It is favorable to treat the problem in the logarithmic τ space. Thus, we look for a fitting solution $y(t)$ in the form:

$$y(t) = \int_0^\infty G(\tau) e^{-t/\tau} d(\log_{10}(\tau)) \quad \forall t \;\; 0 \leqslant t \leqslant \infty, \tag{2}$$

where $G(\tau) = \tau F(\tau) \ln 10$ is the τ spectrum in the $\log_{10}(\tau)$ space.

Through experimental measurements, the evolution of y is sampled in time. Let us assume the vector representation of y sampled at time instances t_i, which are uniformly distributed in logarithmic space between $t_{\min}$ and $t_{\max}$ into M bins. Furthermore, let us discretize Eq. (2) introducing the vector representation of the τ spectrum G and the $(M \times N)$ matrix T containing exponentials with rows corresponding to a time index (denoted by y data) and columns to the τ index,

$$y = GT. \tag{3}$$

Here and in the following the vectors y and G correspond to the discrete representation of the continuous functions $y(t)$ and $G(\tau)$. The elements of matrix T are

$$T_{ij} = e^{-t_i/\tau_j}, \tag{4}$$

where τ_j values are uniformly distributed in the log space in the interval $\tau_{\min} < \tau < \tau_{\max}$ and N is the dimension of the basis used for the inversion of the experimental data. The τ range is uniformly partitioned in N bins and τ_j represents the center of the corresponding bin.

Generally, the τ spectrum can be obtained by computing the inverse matrix T^{-1} as

$$G = T^{-1} y. \tag{5}$$

The inversion is, however, not straightforward due to the properties of the T matrix, which is sparse, generally not square, with a high condition number, i.e., high sensitivity to small variations in the input. The matrix T is sparse since in each row most elements are close to zero because of the nature of the exponential function in the wide range of values of τ needed.

B. Singular value decomposition approach

A robust way to compute the inverse matrix T^{-1} is the SVD, which allows us to control the properties of the inverse matrix by thresholding. The $(M \text{x} N)$ matrix T can be factorized as:

$$T = USV^*, \tag{6}$$

where U is a unitary matrix, S is a diagonal matrix with ordered elements, and V^* is the transposed conjugate of a matrix V. It follows:

$$\begin{aligned} T^{-1} &= VWU^* \\ \hat{G} &= VWU^* y, \end{aligned} \tag{7}$$

where W is a diagonal matrix with dimension N and elements given by

$$W_i = 1/S_{ii}. \tag{8}$$

Derivation of all matrices used in the above equations is a standard calculation [14] and subroutines for SVD are available in most software packages.

C. Thresholding of the diagonal elements of the SVD matrix

The SVD matrix S is a $M \times N$ matrix with nonzero elements only on the diagonal and usually ordered such that $S_{ii} > S_{jj}$ when $i > j$. Most of the elements S_{ii} are close to zero, which leads to huge errors when the computation of $\hat{G}$ from Eq. (7) is performed. Thresholding is thus needed, and it is obtained by setting to zero all elements of W_i with $S_{ii} < s_0$, where s_0 is a defined threshold. The thresholding procedure is equivalent to reducing the number of singular vectors in U and V. An optimal threshold s_0 must therefore be defined to balance between the need of having enough information (sufficient dimension of the singular basis given by the number of nonzero diagonal elements in the SVD matrix) and of filtering contributions determined from noise (numerical or experimental). The relaxation distribution obtained through the SVD approach, $\hat{G}$, depends on the chosen threshold and the properties of time-series data y.

III. ROBUST DETERMINATION OF THE OPTIMAL THRESHOLD

A. Synthetic data

To introduce an optimal and reliable procedure for inverting Eq. (3) [i.e., derive $\hat{F}(\tau)$ from a given dataset], we create synthetic datasets $y(t)$ assuming a known theoretical distribution of relaxation times $F(\tau)$:

$$y(t) = \int_0^\infty F(\tau) e^{-t/\tau} d\tau + n_0 \xi(t). \tag{9}$$

Apart from multirelaxation curve, the dataset contains an additive white noise (which corresponds to the most common noise for experimental data) with noise level n_0, $\xi(t)$ being a

TABLE I. Synthetic data: Chosen theoretical τ spectra. We recall that $G(\tau) = F(\tau)\tau \ln 10$. The corresponding functions are shown in Fig. 1. The parameters chosen for the Weibull distribution are $a = 0.5$ s, $b = -1.5$, and $c = -2.5$. For the rectangular distribution we have $\tau_{\min} = 0.025$ s and $\tau_{\max} = 40$ s.

Case	$F(\tau)$	Equation
A	Weibull	$F(\tau) = \left(\frac{\tau}{a}\right)^b e^{-\left(\frac{\tau}{a}\right)^c}$
B	Rectangular	$F(\tau) = c_0$ for $\tau_{\min} < \tau < \tau_{\max}$
C	Two Weibull	$F(\tau) = \left(\frac{\tau}{a_1}\right)^{b_1} e^{-\left(\frac{\tau}{a_1}\right)^{c_1}} + \left(\frac{\tau}{a_2}\right)^{b_2} e^{-\left(\frac{\tau}{a_2}\right)^{c_2}}$

random function with uniform distribution of values between -1 and 1. Three choices of F are considered (see Table I) and the corresponding time series (without noise) are shown in Fig. 1.

It is noteworthy to recall that determining the distribution of relaxation times is important since it reflects a distribution of features on the microscopic scale of the material, responsible of some physical macroscopic properties, e.g., viscoelastic parameters in macromolecules [9], permeability in sand [17], or the critical spin-glass correlation length in monocrystals [23]. In natural materials, the microscopic spatial scales (grain sizes [20], distribution of contact areas at crack surfaces [39], or pore-sizes [14]) are normally not uniformly distributed and present a most likely dimension (maximum), represented in our study by the Weibull distribution. Artificially made materials (e.g., glass or metal beads [40] or magnetic nanoparticles distributed in a liquid or a gel [41]) are as well originating long-time relaxation processes, but the spatial scale can be precisely controlled and often their uniform distribution (rectangular) is the optimal choice. In some cases, features with distinct spatial scales (e.g., grains and crack [21,42]) might be simultaneously present.

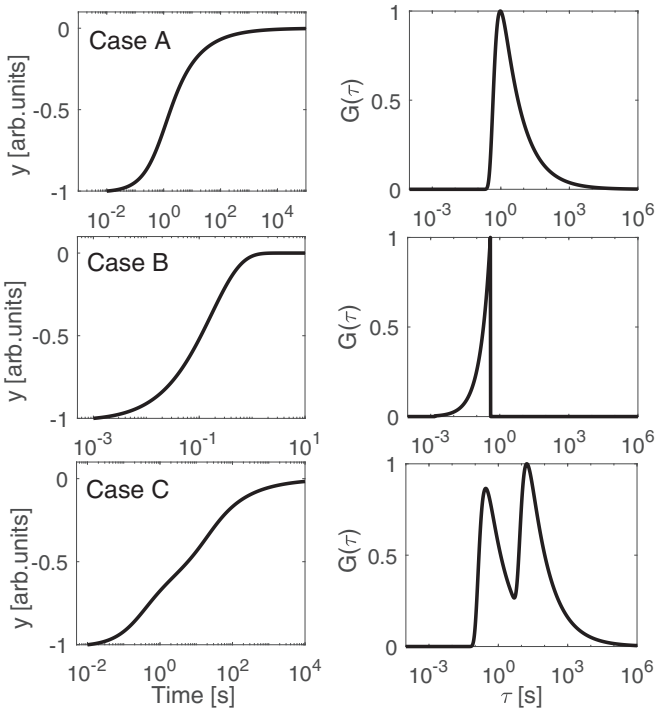

FIG. 1. Left column: Noiseless $y(t)$ functions data used for the analysis shown in the logarithmic time. Right column: Corresponding relaxation distributions $G(\tau)$. Details of the three distributions are reported in Table I.

B. Quantification of the inversion

In order to quantify the results of the inversion procedure, parameters describing the accuracy of τ-spectrum determination and temporal data fitting are introduced. The inversion is performed on synthetic dataset $y(t)$ with the known underlying distribution of relaxation times $G(\tau)$. The result of the inversion according to Eq. (7) is $\hat{G}(\tau)$. The evaluation of $\hat{G}(\tau)$ is dependent on the input data $y(t)$ but also on the threshold level of the approximation of T^{-1}. It is useful to evaluate the resulting fitting curve of the time-series data $\hat{y}(t)$ by substituting $\hat{G}(\tau)$ in Eq. (9).

We quantify the accuracy in reproducing the theoretically expected τ spectrum through the parameter p:

$$p = 1 - r, \tag{10}$$

where r is the Pearson coefficient, a statistical indicator defining the correlation coefficient between expected and reconstructed spectra (G and $\hat{G}$, respectively),

$$r = \frac{\mathrm{cov}(G, \hat{G})}{\sigma_G \sigma_{\hat{G}}}. \tag{11}$$

Here cov denotes the covariance of the theoretical and reconstructed distributions and σ the standard deviation of the corresponding distribution. Note that such a quantity is generally unavailable and will be used here to asses the quality of the inversion.

We also indicate the accuracy of the fit of the temporal evolution $\hat{y}(t)$ introducing the sum of the squared residuals SSR, defined as:

$$\mathrm{SSR} = \sum_{i=1}^{M} (y_i - \hat{y}_i)^2. \tag{12}$$

C. Thresholding effects on the inversion

There is a single parameter controlling the accuracy of the inversed τ spectrum $\hat{G}$ and that is the threshold level s_0 for SVD evaluation of the inverse matrix T^{-1}. The result of the inversion is computed directly from time-series data y which inherently minimizes (for given T^{-1}) the deviation of fitted curve $\hat{y}$ from the input data y quantified by parameter SSR. As will be shown further, the threshold minimizing SSR does not lead to the best approximation of the τ spectrum.

The schematic in Fig. 2 represents the evolution of p and SSR for case A, when input data contains a certain noise level. The representation is fundamentally valid for all cases of underlying distributions. The optimal threshold choice corresponds to that which minimises the corresponding function. However, optimization of the fit of experimental data (SSR) and of the reconstruction of the τ spectrum (p) is not achieved at the same threshold level.

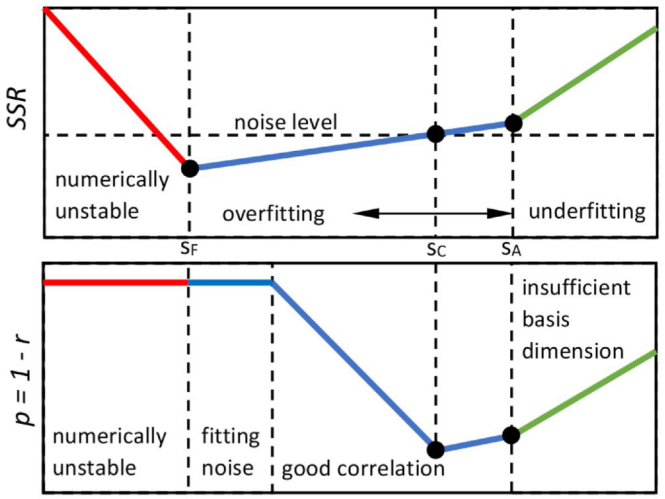

FIG. 2. Schematic representation of the different phases of the inversion procedure. Here SSR (quality of the temporal fit) and p (quality of the correlation of reconstructed and theoretical distributions) are shown as a function of the threshold s_0. Circles represent the threshold values to obtain optimal fit of the data (s_F) and the best correlation of reconstructed and theoretical distributions (s_C). The threshold s_A shown in the plot corresponds to the estimated threshold found with our approach, whose definition will be given later.

The behavior observed in Fig. 2 identifies three regions for both parameters. For very low threshold values (red lines) we have numerical instability resulting in poor performance both in SSR and p. For large threshold values (green lines), the singular basis dimension is strongly reduced and becomes insufficient to provide fit of the data and the τ spectrum. The range of threshold values in between is distinct for SSR and p. The evolution of SSR presents a slightly increasing plateau with the minimum s_F right next to the numerical instability limit. The evolution of p presents a "V"-shaped curve with a narrow range of threshold values resulting in good reconstruction of G.

In Fig. 3 we show the results of the inversion in the aforementioned regions for case A. In the first row ($s_0 < s_F < s_C$) the solution for the τ distribution (right column) is numerically unstable, resulting in a poor fit (although still reasonable) of experimental data (first column). Increasing the threshold to $s_0 = s_F$ (second row), optimal fit of data is obtained, but we still have a bad estimation of $G(\tau)$. This is caused by overfitting, i.e., fitting the relaxation curve $y(t)$ as well as the noise $\xi(t)$. Indeed, as shown in the third row of Fig. 3, for $s_0 = s_C$ optimal reconstruction of $G(\tau)$ is achieved, being the same for the fit of the data. When the threshold is large (fourth row), the singular basis dimension becomes too small and both fit and correlations are poor.

The main issue to be solved is that only the parameter SSR can be quantified in an experiment, as $y(t)$ is known and $G(\tau)$ unknown. The goal, as discussed in the following, is thus to introduce an approach able to estimate the threshold $s_0 = s_C$ from the curve SSR(s_0). Results from inverting synthetic data and corresponding to the schematic representation of Fig. 2 are shown in Figs. 4(a) and 4(b).

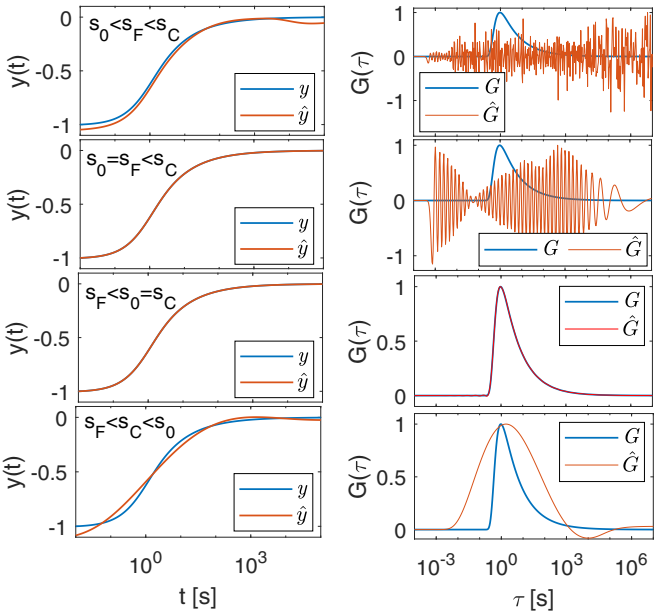

FIG. 3. Dependence of the reconstructed $\hat{y}$ (left column) and τ spectrum ($\hat{G}$) on the threshold level s_0. Data for case A without added noise ($n_0 = 0$) have been inverted.

D. Akaike criterion for the definition of the optimal threshold

When considering the dependence of SSR on the threshold (see Fig. 2), setting aside the numerical instability interval $s_0 < s_F$, it can be separated into two subsets divided by the optimal threshold s_C. For threshold $s_0 < s_C$, the size of singular basis is too high and noise is being fitted by $\hat{y}$, which has the effect of reducing standard deviation SSR beyond the level of

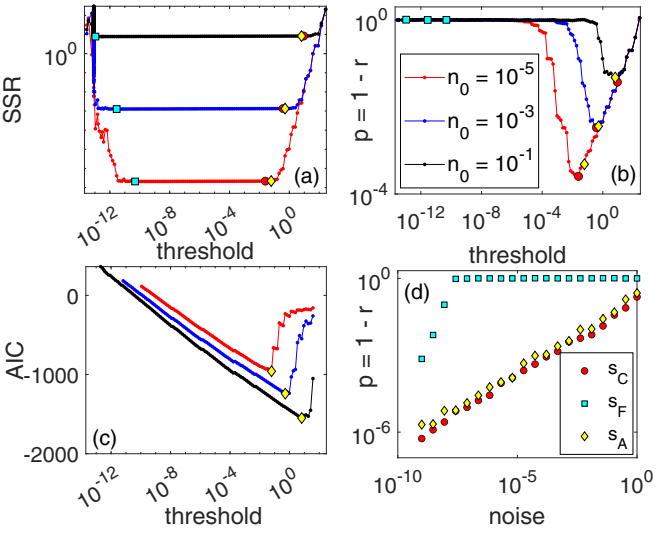

FIG. 4. Estimated optimal threshold using the different approaches described in the text for different noise levels n_0. (a) SSR vs. threshold. (b) p vs. threshold. Symbols in subplots (a) and (b) indicate the estimated optimal threshold from the three approaches. (c) Akaike indicator vs. threshold, the minimum being corresponding to the Akaike threshold s_A. (d) p vs. noise when using thresholds obtained in the three approaches.

additive noise. For threshold $s_0 > s_C$, the size of singular basis is too low, information is being lost and SSR rapidly increases. It will be shown that such transition in SSR(s_0) curve can be detected by the AIC [31–34].

The AIC estimate of the optimal threshold is based on the part of the SSR(s_0) dependence for $s_0 \geqslant s_F$. We consider, that the truncated SSR($s_0 > s_F$) is composed of two subsequent stationary autoregressive (AR) processes. One describing the noise-fitting range of s_0 and the other the underfitting range (see Fig. 2). AIC is a statistical approach allowing us to determine the most probable separation threshold between the two processes.

For the sake of clarity, let us introduce the truncated dependence as the vector x, i.e., $x(j) = \mathrm{SSR}(s_j)$ with $s_F \leqslant s_j \leqslant s_{\max}$, and let us denote the length of x as L. We then split the vector x into two intervals separated by the index k. Let us call $z_1(j) = x(j)$ (for $1 \leqslant j < k$) and $z_2(j) = x(j + k - 1)$ (for $1 \leqslant j \leqslant L - k + 1$). An autoregressive model of the order Q is defined as:

$$z_i(j) = \sum_{q=1}^{Q} a_i(q) z_i(j-q) + e_i(j)$$
$$i = 1, 2; \quad j = Q + 1 : \mathrm{length}(z_i), \tag{13}$$

where $a_i(q)$ are the coefficients of the model and $e_i(j)$ are the nondeterministic parts, for each interval i. We can evaluate the variance $\sigma_i^2(k)$ of the nondeterministic parts (e_i) for a range of separation indexes $k = Q + 1, \ldots, L - Q$. The AIC function can be written as

$$\mathrm{AIC}(k) = (k - Q) \log\left(\sigma_1^2(k)\right) + (L - Q - k) \log\left(\sigma_2^2(k)\right). \tag{14}$$

The minimum of the AIC function corresponds to the optimal separation index between the two stationary AR models, meaning that we get the best fitting of both models in the least-squares sense, i.e., the contribution to fit of the nondeterministic part is minimised. The complex statistical justification is beyond the scope here and can be found in Ref. [43]. The corresponding s_k value gives the AIC estimate of optimal threshold s_A. The results shown here were calculated using the Burg method [44] to estimate AR model coefficients for a fixed model order $Q = 2$. Increasing the model order has no effect on the AIC estimate. The minimum of the AIC function is sharp, as shown in Fig. 4(c) and can be easily identified. The thresholds obtained with this approach are reported as diamond symbols in Figs. 4(a) and 4(b). Data refer to case A (with three noise levels specified in the plots). The thresholds s_F and s_C are reported as squares and circles, respectively.

The Akaike threshold s_A can be determined solely from experimental data and it is equivalent to the optimal threshold s_C, which is unknown for real data. The quality of the distribution of relaxation times obtained using s_A as a threshold is similar to the best achievable with SVD (using the optimal threshold), as shown in Fig. 4(d), where the parameter p is shown as a function of noise for all threshold definitions. In all cases p increases with increasing noise level. The inversion using the AIC allows us to obtain a reconstructed spectrum $\hat{G}$ which is always a good approximation of the best one achievable by the SVD procedure, as will be demonstrated in the next section.

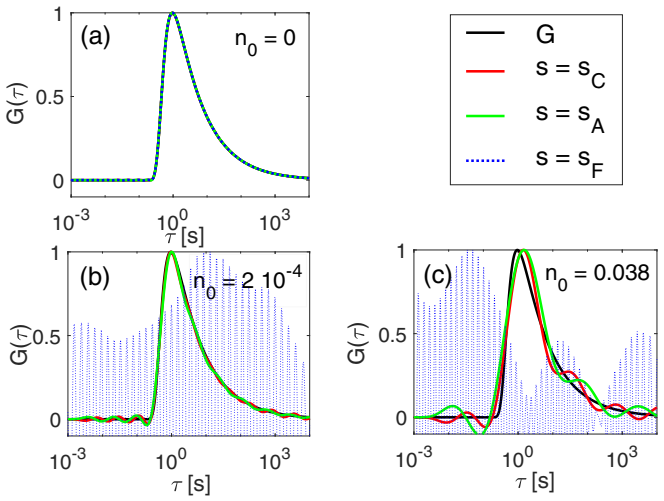

FIG. 5. Reconstructed distribution of relaxation times obtained using different thresholds (case A).

IV. RESULTS

The validity of choosing the Akaike threshold is confirmed when plotting the reconstructed distribution, as shown in Fig. 5. $\hat{G}$ obtained using the Akaike criterion always approximates well the optimal reconstructed distribution, which is evidenced by the values of the Pearson correlation coefficient r in Table II. From now on we refer to inversion results obtained using the SVD approach applied in conjunction with the AIC.

The reconstructed distributions for the three cases reported in Table I are shown in Fig. 6 for two different noise levels. The corresponding Pearson correlation coefficients r are given in Table III. When noise on the inverted data is not present (upper row), the reconstruction is always optimal. Even in the case of a square distribution of relaxation times [Fig. 6(b)], which presents sharp discontinuities, we still get a correlation close to 1. Even low noise levels (results are shown in the right column of Fig. 6) lead to distortions of the reconstructed distributions. The errors in the reconstruction of G increase with the complexity of the distribution function and result in a nonexact determination of the position of the distribution peak. The solution still remains acceptable in terms of r as can be seen in Table III. Also, as mentioned, it is near the optimal solution which could be determined using the SVD approach.

The comparison of results obtained with different approaches, application to invert experimental data and considerations about the empirical robustness of the method are given in Appendices A–C.

TABLE II. Pearson correlation coefficient r for distributions shown in Fig. 5.

Threshold	$n_0 = 0$	$n_0 = 2 \times 10^{-4}$	$n_0 = 0.38$
s_A	0.99	0.998	0.978
s_C	0.999	0.999	0.985
s_F	0.999	0.02	0.001

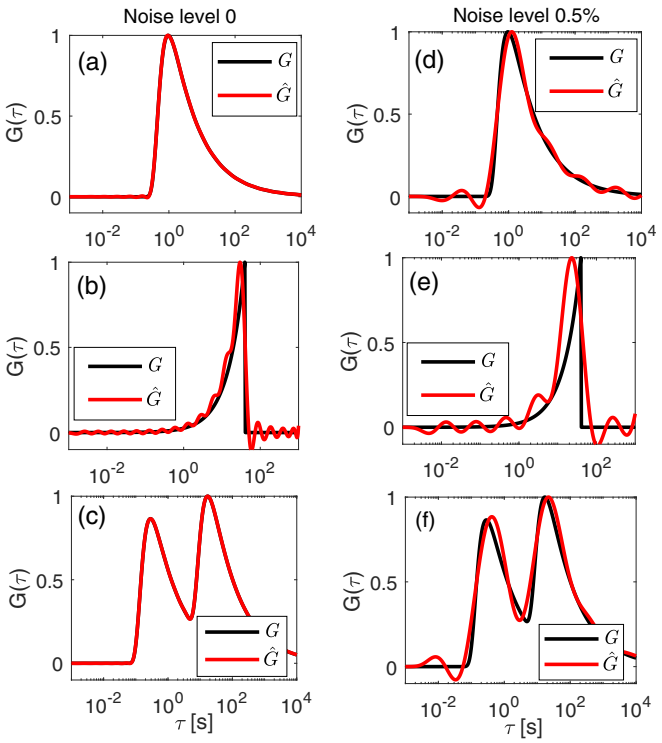

FIG. 6. Reconstructed distribution of relaxation times obtained for the three cases discussed in Table I. Two noise levels have been considered in the two columns.

One of the most important properties of $G(\tau)$ is the most relevant relaxation time τ_m, which is often connected to the dominant microstructural scale (grain size, porosity, etc.). In Fig. 7 we report, as a function of the noise level n_0, the error in the determination of the most relevant relaxation time:

$$\delta\tau_m = (\hat{\tau}_m - \tau_m)/\tau_m. \tag{15}$$

Notice that in the case of the Weibull distribution the most relevant relaxation time corresponds to the most likely relaxation time, i.e., the τ value corresponding to the maximum of $F(\tau)$, while for the rectangular distribution τ_m corresponds to the upper bound of the distribution.

As expected, the Akaike information criterion allows us to obtain errors in the determination of the position of the maximum of $G(\tau)$ comparable to the ones obtained with the optimal criterion. For low noise levels the error is less than 10% for the Weibull distribution. The correctness of the determination of τ_m becomes poor for large noise levels. Experimental conditions in general correspond to noise levels between 10^{-4} and 10^{-2}, where the accuracy for the Weibull distribution is about 20% , which is acceptable considering

TABLE III. Pearson correlation coefficient r for distributions shown in Fig. 6, i.e., for three relaxation times distributions and two noise levels.

$r(s_A)$	Weibull	Uniform	Double Weibull
$n_0 = 0$	0.999	0.954	0.999
$n_0 = 0.005$	0.990	0.889	0.989

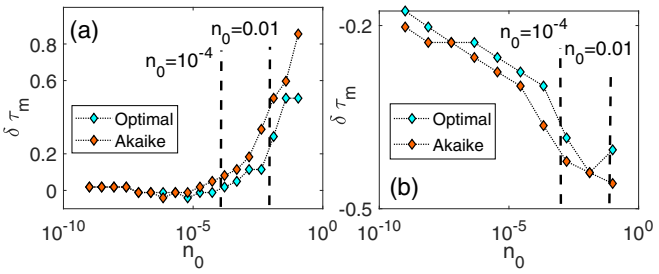

FIG. 7. Accuracy of the approach in determining the most relevant relaxation time [τ value corresponding to the maximum in the distribution function for the Weibull distribution (a) and corresponding to the maximum relaxation time for the rectangular distribution (b)]. We report the error in the estimation of τ_m [see Eq. (15)] as a function of noise level. The typical intervals of the experimental noise level are shown as dashed vertical lines.

that in practical cases the determination of the order of magnitude of the most relevant relaxation time is already of interest.

V. DISCUSSION

As we have discussed so far, the approach proposed allows us to predict a τ spectrum which approximates the best one which can be obtained using the SVD approach. Nevertheless, due to the presence of noise in experimental data, even the best solution is not perfect. Thus, in this section we discuss the limits of reliability of the derived distribution of relaxation times when inverting experimental data (see also an example of inversion in Appendix B). As we will show, a margin of uncertainty in the estimation of the relevant properties of the distribution must always be considered and it could be large under some experimental conditions.

A. Noise level

Experimental data are often affected by noise and here we quantify its effect by considering an additive white noise [see Eq. (9)], which is a good approximation of environmental noise. Multiplicative noise (more related to noise due to the environmental setup) [45] gives similar effects; see Appendix C.

The influence of noise is discussed in Fig. 8. We recall that n_0 is the inverse of the signal-to-noise ratio which in experiments typically is in the range from 10^{-4} to 10^{-2}. From subplot (a) we notice that the thresholding procedure leads to removal of most of the elements of the diagonal SVD matrix W [see Eq. (8)]. Here the fraction of elements of the diagonal SVD matrix which are set to zero is shown and increases significantly with noise [linearly vs. $\log(n_0)$], leading to a loss of information which results in a poorer reconstruction of $G(\tau)$ as is clear in subplot (b): The parameter p increases with noise level, but we still have a cross-correlation with a Pearson coefficient $r = 1 - p \approx 0.995$ for $n_0 = 0.01$ for the two continuous distributions (Weibull and double Weibull), which is close to 1. The situation is worse for the discontinuous distribution (square): $r \approx 0.92$ already for $n_0 = 0.005$. On the contrary, the fit of data ($y(t)$) shows low SSR even for large noise values [Fig. 8(c)], thus further confirming that a good

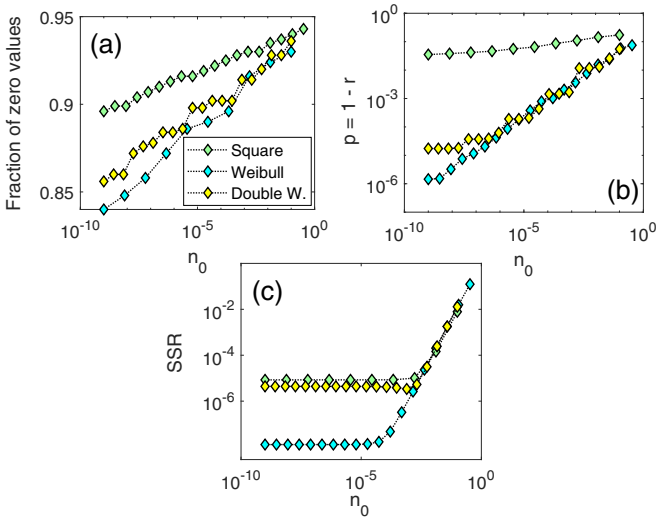

FIG. 8. Effects of noise on the procedure of deriving the time relaxation distribution function. (a) Fraction of elements set to zero in the diagonal SVD matrix; (b) cross-correlation between the reconstructed and expected distribution function ($p = 1 - r$); (c) residuals of the reconstructed and used dataset (SSR). On the x axes we always have the noise level n_0.

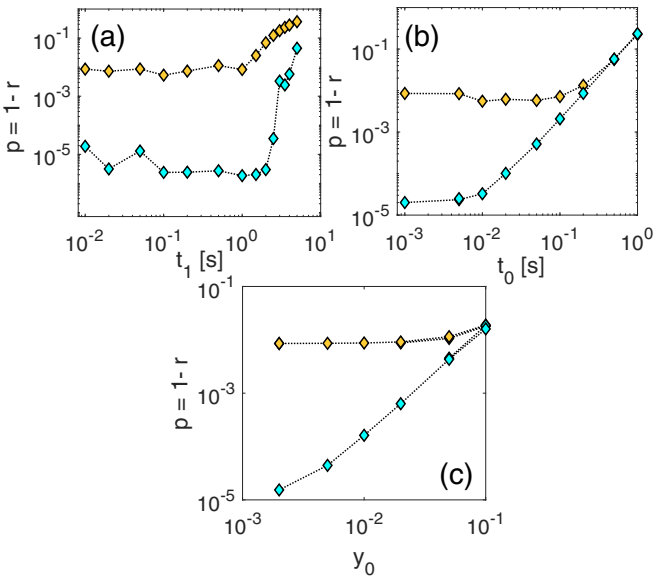

FIG. 9. Effects of incompleteness of the experimental dataset on the reconstruction of the time relaxation distribution function. (a) Effects of missing data for early time relaxation. t_1 indicates the time corresponding to the first data acquisition. (b) Effects of a wrong estimate of the onset time of relaxation (t_0). (c) Effects of a wrong estimate of the asymptotic value of the variable (offset y_0 in the data). In all plots, data for exact (cyan symbols) and noisy (red symbols) data are reported. Noise was $n_0 = 0.005$.

data fit does not always correspond to a correct reconstruction of $G(\tau)$.

B. Incompleteness of the dataset

Experimental datasets are often incomplete, either because early data are not accessible (due to the intrinsic time needed for the acquisition) or because experiments are stopped before reaching the final equilibrium state. In order to simulate these situations and analyze their influence on the reconstruction of the distribution of relaxation times, we have considered case A of Table I (Weibull distribution of the relaxation times) and built incomplete datasets as:

$$y(t) = \int_0^\infty G(\tau) e^{-t/\tau} d(\log_{10}(\tau)) \quad t_1 \leqslant t \leqslant t_2. \tag{16}$$

Refer to Fig. 1(a) for a plot of the complete dataset and the timescales present. First [Fig. 9(a)] we consider the case in which $t_2 \to \infty$ and analyze the reconstructed relaxation times distribution as a function of t_1. To quantify the quality of the reconstruction of $G(\tau)$ we use again the indicator p defined in Eq. (10), related to the cross-correlation of the reconstructed distribution with the theoretical one. The accuracy of the reconstructed $G(\tau)$ remains constant increasing t_1 up to almost 1 s [both in the case of noisy (red) and not noisy (cyan) data]. Thus, we still obtain $r \gg 0.99$ up to when the experimental data covers at least a portion of the time region $t < \tau_m$ [see Fig. 1(a) where τ_m is the most likely relaxation time]. Later, the performances of the approach decrease with increasing t_1.

We also observed that p does not depend on t_2, that is, the incompleteness of the datasets at late times is not relevant (not shown).

Two additional issues are to be considered when dealing with experimental data:

(i) $y_{\rm exp}(t) = y(t - t_0)$. The onset time of relaxation is often difficult to define or measure accurately. It follows that experimental timescale is affected by an error which could be as large as the time corresponding to the first data acquisition, resulting in a time shift of the dataset given by the variable t_0 above and corresponding to the lag between estimated and real time of onset of relaxation effects;

(ii) $y_{\rm exp}(t) = y(t) + y_0$. Often y is measured as a variation with respect to an asymptotic equilibrium value ($t \to \infty$). The uncertainties in the estimation of the equilibrium position leads to an offset of the measured signal y_0.

The influence of t_0 and y_0 on the reconstruction of $G(\tau)$ is shown in Figs. 9(b) and 9(c), respectively. In the case of noiseless data (cyan symbols) the quality of the reconstruction of G decreases steadily with increasing t_0 or y_0. For noisy data (red symbols) the uncertainties in the experimental determination of onset relaxation time and offset are mostly smaller than uncertainties due to noise (the parameter p is almost independent from t_0 and y_0 and starts increasing only for large values of t_0 and only slightly for y_0). The approach thus still works reasonably well in the cases of interest on practice, where $t_0 << \tau_m$, i.e., $t_0 \leqslant 1$ s ($r = 1 - p > 0.99$). More critical from the experimental point of view is the determination of the offset, for which errors up to 10 or 20% can be easily reached, having thus a considerable influence on the reconstruction of G.

C. Peak detection and resolution

In this subsection we analyze the efficiency of the approach in resolving the presence of more than one peak in the

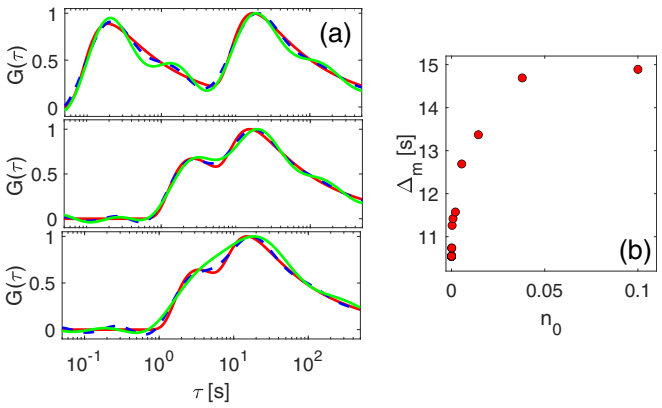

FIG. 10. Resolution accuracy: (a) Examples of double Weibull distributions used for the analysis for three values of resolution parameter (distance between peaks): Red solid lines are the theoretical distributions while dashed blue and solid green lines represent the reconstructed distributions in the absence and in the presence of noise ($n_0 = 0.005$), respectively. (b) Minimum peak distance detectable with the proposed approach as a function of noise level.

τ spectrum. To this purpose, we have considered the case of a double Weibull distribution, when two peaks are present: τ_m^1 and τ_m^2. The position of the peak corresponding to the lower relaxation time is modified and we introduce the resolution parameter $\Delta = \tau_m^2 - \tau_m^1$. Examples of the distributions are reported in Fig. 10(a). While the presence of the two peaks is always discernible in the theoretical distributions (red solid lines) and in the reconstructed distribution when there is no noise (blue dashed line), this is not the case when noise is present (green curve refers to the case of $n_0 = 0.005$).

The resolution parameter Δ_m, i.e., the minimum distance between peaks which can be detected [as shown in Fig. 10(b)] decreases significantly with increasing noise. We remark that the presence of the lowest peak was indistinguishable already in the theoretical solution for $\Delta < 10.5$ s.

VI. CONCLUSIONS

The inversion of noisy experimental data of long-time relaxation processes to obtain a spectrum of relaxation times is an ill-posed problem with a nonunique solution. The inversion using SVD approach allows us to find an approximate solution based on a certain threshold value. The criterion often adopted of determining the threshold as the one which allows best fitting of experimental data is often far from being satisfactory and the optimal fit of the data does not always correspond to the optimal reconstruction of the τ spectrum. We have shown here on controlled synthetic data that an optimal threshold of the SVD inversion exists and that it is strongly dependent on the properties of the dataset. By combining the SVD inversion with the Akaike information criterion, a solution which approximates the optimal one can be reached without any *a priori* knowledge about the spectrum.

Despite the approach discussed here has advantages with respect to other approaches proposed in the literature, still the obtained distribution of relaxation times could be regarded as only a qualitative approximation of the real solution. Indeed, as shown here inverting synthetic data, the quality of the correlation between the expected solution and the one found inverting data decreases rapidly with increasing noise. When the signal-to-noise ratio is good (noise level <0.005), as in most experiments, results of the inversion procedure proposed here could provide quantitatively meaningful results. For higher noise levels, only a general agreement of the distribution shape and the order of magnitude of the most relevant relaxation time can be inferred.

However, despite the fact that our results confirm the existence of critical issues, the possibility with the proposed approach to obtain a qualitative description of the distribution of relaxation times and discriminate between distributions with one or two peaks or with a given asymmetry is fundamental in view of solving the problem. Indeed, the solution found combining AIC and SVD suggests a plausible model of the distribution, at least in terms of asymmetry and presence of maxima. Therefore, our approach allows us to obtain from data (as opposed to *a priori* hypotheses) some information which allows us to simplify the problem and reducing it to determining a few parameters (those defining the distribution) by fitting experimental data. As shown elsewhere, postulating a suitable analytical form for the solution works well in practice, giving accurate information about the main features of the distribution: determination of the most relevant relaxation time, width of the distribution, asymmetry, and relaxation times range [9,20].

ACKNOWLEDGMENTS

This research was funded by Centre of Excellence for Nonlinear Dynamic Behaviour of Advanced Materials in Engineering (Grant No. *CZ*.02.1.01/0.0/0.0/15_003/0000493 of the European Structural and Investment Funds, Operational Programme Research, Development and Education of the European Union). J.K. and D.G. claim institutional support (RVO: 61388998).

APPENDIX A: COMPARISON WITH OTHER METHODS

Other methods have been proposed in the literature as a solution to the long-time relaxation inversion. Here a comparison of a method based on SVD inversion and on multirelaxation fitting will be given.

For what concerns SVD, a solution for determining the optimal threshold consists in iteratively repeating the SVD approach to eliminate all negative values of the solution, which are not physical [13]. In practice, starting with a full matrix T, a tentative solution G is computed. If all components are nonnegative, then the solution is accepted. Otherwise, the column of T corresponding to the least amplitude is eliminated and a reduced matrix T' obtained. The corresponding component in G is set to zero and also eliminated to form a reduced vector G'. The procedure is repeated iteratively up to convergence.

This procedure was applied to invert synthetic data (case A with a low noise $n_0 = 0.001$). Results are reported in the second row of Fig. 11 and compared with the results obtained with our approach (first row). In Fig. 11(e), we report as dashed lines $\tilde{G}$ obtained for two different choices of the initial matrix T (i.e., the choice of the range of τ values used for the inversion). The two cases refer to the choices 10^{-4} s <

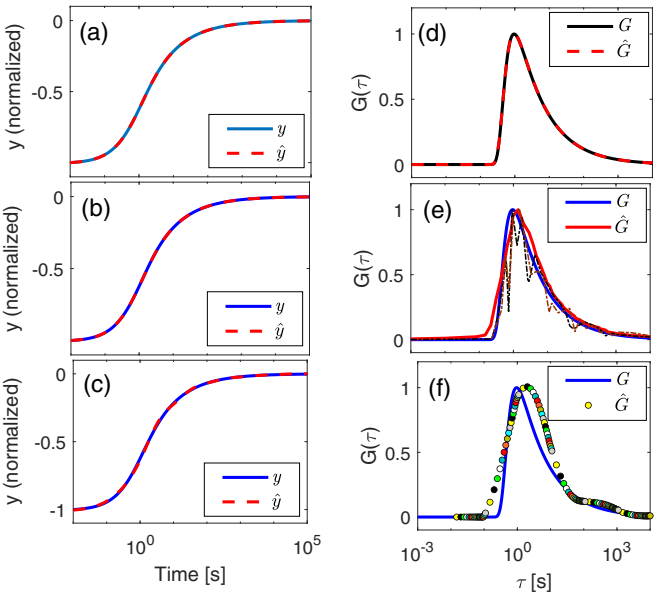

FIG. 11. Inversion using different approaches. Case A with small noise ($n_0 = 0.001$). First column: y vs. t. Second column: distribution of relaxation times vs. τ. [(a) and (d)] SVD + AIC approach; [(b) and (e)] SVD with zeros elimination; [(c) and (f)] inversion fitting with a discrete number of exponentials.

$\tau < 10^6$ s and 10^{-5} s $< \tau < 10^5$ s, respectively. Each solution reconstructs part of the theoretical distribution (blue solid line), but they are sensitive to the inversion parameters. Averaging solutions for different choices of the matrix T is thus necessary. The result averaging over 20 realizations is shown as a red solid line and fits the theoretical distribution with a Pearson coefficient $r = 0.982$. Despite that the quality of fit is comparable to that obtained with our approach [compare Fig. 11(a) and 11(b)], the SVD+AIC approach gives a better reconstruction of the distribution [Fig. 11(d), with $r = 0.999$].

An alternative consists in fitting data with the sum of a finite number of exponentials [19]. A basis of relaxation times is defined $B = \{B_1, B_2, \ldots B_N\}$, where $B_i = \log_{10}(\tau_i)$ with elements equally spaced in the $\log(\tau)$ space. It follows:

$$\hat{y} = \sum_{i=1}^{N} G_i e^{-t/10^{B_i}}, \tag{A1}$$

where the coefficients G_i can be derived by fitting the experimental data. By adopting different choices for B_1 and inverting independently for each choice, an ensemble of sets of coefficients G_i could be determined, leading to a continuous spectrum of values.

The results of the application of the procedure to the same synthetic data of the previous case are shown as circles in Fig. 11(f). Here we used $N = 6$ and repeated the calculation for 20 choices of the basis (different colors). The resulting spectrum approximates the expected solution (blue line). The quality of the fit of $y(t)$ [Fig. 11(c)] is the same as that obtained using the two SVD approaches, but the solution for $\hat{G}$ is not good, even though the main features are captured: Position and presence of a single peak, width of the distribution and asymmetry.

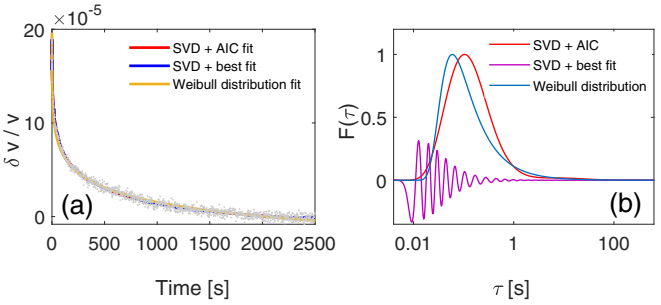

FIG. 12. Inversion of experimental data. (a) Experimental data and fitting functions; (b) distribution of relaxation times.

APPENDIX B: INVERSION OF EXPERIMENTAL DATA

We have applied our approach to experimental data, measured for a specific physical system: elastic slow dynamics (and in particular its relaxation phase), which is a typical long-time process observed in consolidated granular media which manifest hysteresis in their elastic response [20,46,47]. Experimental observations consist in measuring the temporal evolution of the elastic wave velocity, using a low-amplitude perturbation wave (probe). At a certain time, the sample is perturbed with a large-amplitude excitation and conditioning is observed: Velocity drops and a new equilibrium is reached. As soon as the perturbing strain is removed, velocity increases and slowly in time recovers its original value, i.e., the phenomenon is fully reversible. The latter part of the experiment is called relaxation and it is of interest here.

In Fig. 12 we show the temporal evolution of the relative variation of velocity in Berea sandstone after conditioning the sample for three minutes. Details of the experimental procedure used to measure velocity and to condition the sample can be found in Ref. [20]. The fitting solution approximates well the experimental data, as shown in Fig. 12(a). The obtained distribution of relaxation times is reported as a red solid line in Fig. 12(b). The solution without introducing the AIC criterion for the determination of the threshold is also shown (magenta). This solution fits well experimental data, but the negative values in $\hat{G}$ makes the solution not physical.

The distribution obtained with our approach [red line in Fig. 12(b)] can be compared with that obtained using the approach discussed in Refs. [20,21] (blue line), where a function describing the distribution of relaxation times is postulated and the parameters of the function are derived fitting data using the integral expression of Eq. (1). The distribution obtained with the SVD+AIC approach and that obtained postulating a functional form for the distribution (Weibull) are different, but the agreement between the two results is satisfactory: In both approaches we obtain an asymmetric distribution with one peak and comparable widths, while the most relevant relaxation time (related here to the grain size of Berea [20]) is found to be of the same order of magnitude.

APPENDIX C: ROBUSTNESS

The SVD approach combined with the AIC criterion for the determination of the threshold was shown in the main text to provide solutions which always approximates well the optimal

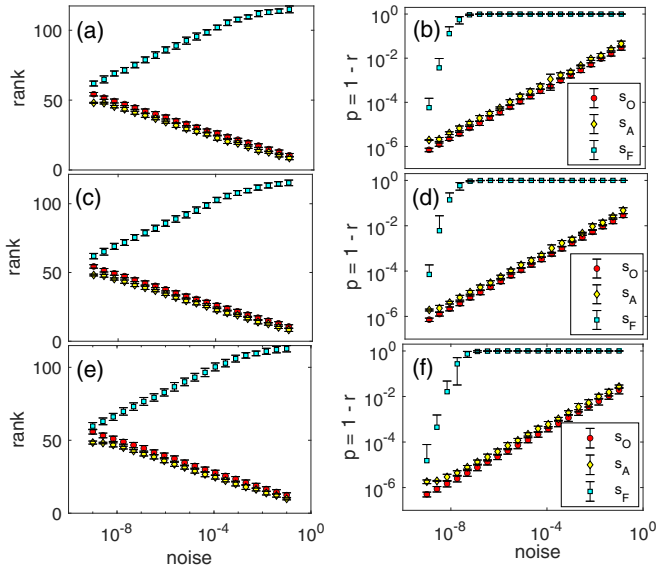

FIG. 13. Robustness of the approach. Left column: Rank of the solution as a function of noise for the three choices of the threshold. Right column: Correlation between predicted and theoretical distributions defined by $p = 1 - r$ vs. noise. [(a) and (b)] Results are obtained averaging solutions obtained inverting the same set of data but changing the range of τ values over which the solution is searched. [(c) and (d)] Results are obtained averaging solutions obtained inverting the same set of data with different noise realizations. [(e) and (f)] Results are obtained averaging solutions obtained inverting the same set of data with different multiplicative noise realizations (dynamic noise).

one. Here we further discuss the "empirical" robustness of the approach, i.e., we analyze its performances with respect to the choice of the parameters of the SVD inversion (dimension of matrix T and range of τ values) and to the presence and type of noise.

The SVD approach is based on defining a basis of exponential functions in the form of a matrix M. In doing so, implicitly a basis (dimension and range) for the relaxation times is chosen: $\tau_{\min} < \tau < \tau_{\max}$. We have analyzed the influence on the solution of this arbitrary choice of the range of the bases (varying $\tau_{\min}$ and $\tau_{\max}$ but maintaining a fixed dimension). The rank of the solution (i.e., number of zero elements of the matrix W) and the indicator p have been calculated for each solution. The average values are shown in Figs. 13(a) and 13(b). Independently on noise level, results are highly repeatable (small error bars), thus confirming the procedure to be independent from the parameters used for the inversion.

In real-world experiments, when repeating the experiment the underlying distribution of relaxation times $G(\tau)$ remains the same but the noise realization is different. Results to verify the "empirical" robustness of the approach vs. noise are shown in Figs. 13(c) and 13(d). The inversion was repeated 120 times using data generated by the same deterministic component and different noise functions. The obtained rank and p values are averaged independently for each noise level. The small error bars indicate that a consistent quality of inversion is obtained independently from noise details (provided it has a given amplitude).

Finally, other noise types might be affecting the quality of experimental data. Among them, dynamical noise might be present. A simple way to simulate dynamical noise is replacing additive noise in Eq. (9) with a multiplicative noise:

$$y(t) = \int_0^\infty F(\tau) e^{-t/\tau} d\tau \times [1 + n_0 \xi(t)]. \qquad \text{(C1)}$$

Results for rank and p (averaging over 120 noise realizations) are reported in Figs. 13(e) and 13(f). Conclusions are similar to the previous case (with only minor variations in the correlation p), confirming robustness with respect to noise type.

[1] R. A. Guyer, J. A. Ten Cate, and P. A. Johnson, Hysteresis and the Dynamic Elasticity of Consolidated Granular Materials, Phys. Rev. Lett. **82**, 3280 (1999).

[2] M. Scalerandi, C. Mechri, M. Bentahar, A. Di Bella, A. S. Gliozzi, and M. Tortello, Experimental Evidence of Correlations Between Conditioning and Relaxation in Hysteretic Elastic Media, Phys. Rev. Appl. **12**, 044002 (2019).

[3] M. Scalerandi, M. Bentahar, and C. Mechri, Conditioning and elastic nonlinearity in concrete: Separation of damping and phase contributions, Construct. Build. Mater. **161**, 208 (2018).

[4] A. Cuetos and A. Patti, Dynamics of hard colloidal cuboids in nematic liquid crystals, Phys. Rev. E **101**, 052702 (2020).

[5] D. Cywiak, A. Gil-Villegas, and A. Patti, Long-time relaxation dynamics in nematic and smectic liquid crystals of soft repulsive colloidal rods, Phys. Rev. E **105**, 014703 (2022).

[6] P. Ilg, Equilibrium magnetization and magnetization relaxation of multicore magnetic nanoparticles, Phys. Rev. B **95**, 214427 (2017).

[7] K. Niss, J. C. Dyre, and T. Hecksher, Long-time structural relaxation of glass-forming liquids: Simple or stretched exponential? J. Chem. Phys. **152**, 041103 (2020).

[8] C. K. Mishra, X. G. Ma, P. Habdas, and K. B. Aptowicz, Correlations between short- and long-time relaxation in colloidal supercooled liquids and glasses, Phys. Rev. E **100**, 020603(R) (2019).

[9] M. Kraft, J. Meissner, and J. Kaschta, Linear viscoelastic characterization of polymer melts with long relaxation times, Macromolecules **32**, 751 (1999).

[10] S. H. Chen, C. P. Broedersz, T. Markovich, and F. C. MacKintosh, Nonlinear stress relaxation of transiently crosslinked biopolymer networks, Phys. Rev. E **104**, 034418 (2021).

[11] M. Tong, L. Li, W. Wang, and Y. Jiang, Determining capillary-pressure curve, pore-size distribution, and permeability from induced polarization of shaley sand, Geophysics **71**, N33 (2006).

[12] J. Rivière, P. Shokouhi, R. A. Guyer, and P. A. Johnson, A set of measures for the systematic classification of the nonlinear

elastic behavior of disparate rocks, J. Geophys. Res. Solid Earth **120**, 1587 (2015).
[13] M. Tong, L. Li, W. Wang, and Y. Jiang, A time-domain induced-polarization method for estimating permeability in a shaly sand reservoir, Geophys. Prospect. **54**, 623 (2006).
[14] N. Florsch, C. Camerlynck, and A. Revil, Direct estimation of the distribution of relaxation times from induced-polarization spectra using a Fourier transform analysis, Near Surf. Geophys. **10**, 517 (2012).
[15] K. Titov, V. Komarov, V. Tarasov, and A. Levitski, Theoretical and experimental study of time domain-induced polarization in water-saturated sands, J. Appl. Geophys. **50**, 417 (2002).
[16] L. Ostrovsky, A. Lebedev, J. Riviere, P. Shokouhi, C. Wu, M. A. Stuber Geesey, and P. A. Johnson, Long-time relaxation induced by dynamic forcing in geomaterials, J. Geophys. Res. Solid Earth **124**, 5003 (2019).
[17] D. Finck, C. Seidel, J. Hausmann, and T. Rief, Creep-induced screw preload loss of carbon-fiber sheet molding compound at elevated temperature, Materials **12**, 3598 (2019).
[18] M. Tokuyama, Slow dynamics in glass-forming materials at alpha- and beta-relaxation stages based on time-convolutionless mode-coupling theory, Physica A **289**, 57 (2001).
[19] P. Shokouhi, J. Rivière, R. A. Guyer, and P. A. Johnson, Slow dynamics of consolidated granular systems: Multi-scale relaxation, Appl. Phys. Lett. **111**, 251604 (2017).
[20] J. Kober, A. S. Gliozzi, M. Scalerandi, and M. Tortello, Material Grain Size Determines Relaxation-Time Distributions in Slow-Dynamics Experiments, Phys. Rev. Appl. **17**, 014002 (2022).
[21] J. Kober, A. Kruisova, and M. Scalerandi, Elastic slow dynamics in polycrystalline metal alloys, Appl. Sci. **11**, 8631 (2021).
[22] A. Tarasov and K. Titov, Relaxation time distribution from time domain induced polarization measurements, Geophys. J. Int. **170**, 31 (2007).
[23] G. G. Kenning, D. L. Schlagel, and V. Thompson, Experimental determination of the critical spin-glass correlation length in single-crystal CuMn, Phys. Rev. B **102**, 064427 (2020).
[24] S. Nordsiek and A. Weller, A new approach to fitting induced-polarization spectra, Geophysics **73**, F235 (2008).
[25] R. Snieder, C. Sens-Schönfelder, and R. Wu, The time dependence of rock healing as a universal relaxation process, a tutorial, Geoph. J. Int. **208**, 1 (2017).
[26] J. C. Nash, A one-sided transformation method for the singular value decomposition and algbraic eigenproblem, Comput. J. **18**, 74 (1975).
[27] Z. Y. Xie, J. Chen, M. P. Qin, J. W. Zhu, L. P. Yang, and T. Xiang, Coarse-graining renormalization by higher-order singular value decomposition, Phys. Rev. B **86**, 045139 (2012).
[28] Y. L. Zou *et al.*, Inversion of nuclear magnetic resonance echo data based on maximum entropy, Geophysics **81**, D1 (2016).
[29] G. Landi, F. Zama, and V. Bortolotti, A new hybrid inversion method for 2D nuclear magnetic resonance combining TSVD and Tikhonov regularization, J. Imag. **7**, 18 (2021).
[30] Zhang Dang, L. V. Yong. L. Yurong, and Y. Cancan, Optimized dynamic mode decomposition via non-convex regularization and multiscale permutation entropy, Entropy **20**, 152 (2018).
[31] H. Akaike, Information theory and an extension of the maximum likelihood principle, in, *Proceedings of the 2nd International Symposium on Information Theory*, edited by B. N. Petrov and F. Csaki (Springer-Verlag, Berlin, 1973), p. 26781.
[32] A. Carpinteri, J. Xu, G. Lacidogna, and A. Manuello, Reliable onset time determination and source location of acoustic emissions in concrete structures, Cement Concr. Compos. **34**, 529 (2012).
[33] J. Y. Zhang, L. L. Dong, and N. W. Xu, Noise suppression of microseismic signals via adaptive variational mode decomposition and Akaike information criterion, Appl. Sci. **10**, 3790 (2020).
[34] J. H. Kurz, C. U. Grosse, and H. W. Reinhardt, Strategies for reliable automatic onset time picking of acoustic emissions and of ultrasound signals in concrete, Ultrasonics **43**, 538 (2005).
[35] S. Zhao *et al.*, Estimating the serial interval of the novel coronavirus disease (COVID-19): A statistical analysis using the public data in Hong Kong from January 16 to February 15 2020, Front. Phys. **8**, 347 (2020).
[36] P. Moeck, On classification approaches for crystallographic symmetries of noisy 2D periodic patterns, IEEE Trans. Nanotechnol. **18**, 1166 (2019).
[37] C. Lu, R. Danzer, and F. D. Fisher, Fracture statistics of brittle materials: Weibull or normal distribution, Phys. Rev. E **65**, 067102 (2002).
[38] Y. Cheng, Y. B. Jin, Y. K. Zhou, T. Hao, and Y. Li, Distinction of Acoustically Induced Transparency and Autler-Townes Splitting by Helmholtz Resonators, Phys. Rev. Appl. **12**, 044025 (2019).
[39] N. Pugno, F. Bosia, A. S. Gliozzi, P. P. Delsanto, and A. Carpinteri, Phenomenological approach to mehcanical damage-growth analysis, Phys. Rev. E **78**, 046103 (2008).
[40] J. Y. Yoritomo and R. Weaver, Slow dynamic elastic recovery in unconsolidated metal structures, Phys. Rev. E **102**, 012901 (2020).
[41] A. A. Kuznetsov, A. V. Novak, E. S. Pyanzina, and S. S. Kantorovich, Structural and magnetic equilibrium properties of a semi-dilute suspension of magnetic multicore nanoparticles, J. Mol. Liq. **359**, 119373 (2022).
[42] J. B. Legland, Y. Zhang, O. Abraham, O. Durand, and V. Turnat, Evaluation of crack status in a meter-size concrete structure using the ultrasonic nonlinear coda wave interferometry, J. Acoust. Soc. Am. **142**, 2233 (2017).
[43] R. Sleeman and T. van Eck, Robust automatic P-phase picking: An on-line implementation in the analysis of broadband seismogram recordings, Phys. Earth Planet. Inter. **113**, 265 (1999).
[44] J. P. Burg, A new analysis technique for time series data, in *Modern Spectrum Analysis*, edited by D. G. Childers (IEEE Press, New York, 1968).
[45] M. Bentahar, R. El Guerjouma, S. Idijmarene, and M. Scalerandi, Influence of noise on the threshold for detection of elastic nonlinearity, J. Appl. Phys. **113**, 043516 (2013).
[46] J. A. TenCate, E. Smith, and R. A. Guyer, Universal Slow Dynamics in Granular Solids, Phys. Rev. Lett. **85**, 1020 (2000).
[47] M. Scalerandi, A. S. Gliozzi, C. L. E. Bruno, and P. Antonaci, Nonequilibrium and hysteresis in solids: Disentangling conditioning from nonlinear elasticity, Phys. Rev. B **81**, 104114 (2010).